Available online at www.sciencedirect.com
ScienceDirect
Geochimica et Cosmochimica Acta 70 (2006) 4151–4165
Geochimica
www.elsevier.com/locate/gca

Sorption of yttrium and rare earth elements by amorphous ferric hydroxide: Influence of solution complexation with carbonate

Kelly A. Quinn, Robert H. Byrne *, Johan Schijf [1]

College of Marine Science, University of South Florida, 140 7th Avenue South, St. Petersburg, FL 33701, USA

Received 7 February 2006; accepted in revised form 13 June 2006

Abstract

The influence of solution complexation on the sorption of yttrium and the rare earth elements (YREEs) by amorphous ferric hydroxide was investigated at 25 °C over a range of pH (4.0–7.1) and carbonate concentrations (0 M $\leqslant [CO_3^{2-}]_T \leqslant$ 150 μM). Distribution coefficients, defined as ${}_iK^T_{Fe} = [MS_i]_T/(M_T \times [S_i])$, where $[MS_i]_T$ is the total concentration of sorbed YREE, M_T is the total YREE concentration in solution, and $[S_i]$ is the concentration of amorphous ferric hydroxide, initially increased in magnitude with increasing carbonate concentration, and then decreased. The initial increase of ${}_iK^T_{Fe}$ is due to sorption of YREE carbonate complexes (MCO_3^+), in addition to sorption of free YREE ions (M^{3+}). The subsequent decrease of ${}_iK^T_{Fe}$, which is more extensive for the heavy REEs, is due to the increasing intensity of YREE solution complexation by carbonate ions. The competition for YREEs between solution complexation and surface complexation was modeled via the equation:

$$ {}_iK^T_{Fe} = \frac{({}_S\beta_1[H^+]^{-1} + {}_S\beta_2[H^+]^{-2} + {}^{CO_3}_{S}\beta_1 \times {}^{H}_{CO_3}\beta_1[HCO_3^-]_T[H^+]^{-2})}{({}_SK_1[H^+] + 1) \times (1 + {}_{HCO_3}\beta_1[HCO_3^-]_T + {}^{H}_{CO_3}\beta_1[HCO_3^-]_T[H^+]^{-1} + {}^{H}_{CO_3}\beta_2[HCO_3^-]^2_T[H^+]^{-2})} $$

where ${}_S\beta_1$ and ${}_S\beta_2$ are equilibrium constants for free YREE surface species, ${}^{CO_3}_{S}\beta_1$ is the equilibrium constant for the YREE-carbonate surface species, ${}_SK_1$ is the surface protonation constant for amorphous ferric hydroxide, and ${}_{HCO_3}\beta_1$, ${}^{H}_{CO_3}\beta_1$, and ${}^{H}_{CO_3}\beta_2$ are YREE solution complexation constants expressed in terms of bicarbonate concentrations. The equation, which includes (i) a single new constant (${}^{CO_3}_{S}\beta_1$) for each YREE, (ii) previously published sorption coefficients (${}_S\beta_1$ and ${}_S\beta_2$) determined in the absence of carbonate, and (iii) previously published solution complexation constants, precisely predicts both the absolute magnitude of ${}_iK^T_{Fe}$ and the pattern of ${}_iK^T_{Fe}$ values over our range of experimental conditions. Experimentally observed ${}_iK^T_{Fe}$ values, spanning more than five orders of magnitude, are accurately described by our surface/solution complexation model. The $\log {}^{CO_3}_{S}\beta_1$ values determined for each YREE in this work are: Y(-1.30 ± 0.04), La(-0.39 ± 0.02), Ce(-0.21 ± 0.02), Pr(-0.22 ± 0.02), Nd(-0.20 ± 0.02), Sm(-0.20 ± 0.02), Eu(-0.26 ± 0.02), Gd(-0.38 ± 0.02), Tb(-0.40 ± 0.02), Dy(-0.51 ± 0.02), Ho(-0.57 ± 0.02), Er(-0.59 ± 0.02), Tm(-0.56 ± 0.02), Yb(-0.62 ± 0.02), and Lu(-0.59 ± 0.02).

1. Introduction

It is generally recognized that distributions of yttrium and the rare earth elements (YREEs) in the ocean are controlled by competition between solution complexation and surface complexation. Since YREE solution chemistry has been relatively well characterized (see for instance Wood, 1990; Byrne and Sholkovitz, 1996), recent studies of YREE

* Corresponding author. Fax: +1 727 553 1189.
E-mail address: byrne@marine.usf.edu (R.H. Byrne).
[1] Present address: Chesapeake Biological Laboratory, University of Maryland Center for Environmental Science, P.O. Box 38, Solomons, MD 20688, USA.

0016-7037/$ - see front matter © 2006 Elsevier Inc. All rights reserved.
doi:10.1016/j.gca.2006.06.014

fractionation processes have focused on YREE surface chemistry. Early investigations of REE sorption in seawater utilized radiotracers and a variety of substrates, both organic (Bingler et al., 1989; Byrne and Kim, 1990; Stanley and Byrne, 1990) and inorganic (Byrne and Kim, 1990; Koeppenkastrop et al., 1991). These studies showed that for most substrates, light REEs (LREEs) are preferentially removed from seawater compared to heavy REEs (HREEs). Silica phases, which displayed a greater affinity for HREEs (Byrne and Kim, 1990), were an exception to this generality. The major limitation of these early YREE sorption investigations was the omission of many REEs whose radionuclides were too short-lived or not commercially available. Toward a more comprehensive view of YREE sorption in seawater, Koeppenkastrop and De Carlo (1992) examined sorption of all REEs, except Pm and Sm, onto amorphous ferric hydroxide and crystalline FeOOH. Despite more extensive sorption by the amorphous phase, the crystalline phase produced stronger fractionation and a residual seawater pattern that resembled shale-normalized REE patterns in the ocean (Koeppenkastrop and De Carlo, 1992).

As noted by Koeppenkastrop and De Carlo (1992), interpretation of experiments performed in seawater is complicated by the presence of strong solution complexation. As such, it was recognized that experiments should be undertaken in simple synthetic media in the absence of strongly complexing ligands. Starting with the work of De Carlo et al. (1998), (Y)REE sorption onto amorphous ferric hydroxide in simple synthetic solutions (without complexing ligands) has been investigated over a range of pH (4.0–9.0) and ionic strength (0–0.7 M) (Bau, 1999; Kawabe et al., 1999a; Ohta and Kawabe, 2001; Quinn et al., 2004, 2006). In general these experiments showed that, in the absence of solution complexation, sorption does not preferentially remove LREEs from solution. Quinn et al. (2004) showed that the YREE pattern obtained in experiments at near-neutral pH closely resembles the sorption pattern of natural marine particles that is predicted (Byrne and Sholkovitz, 1996) using shale-normalized oceanic YREE concentrations and a quantitative model of YREE solution complexation in seawater.

It has been well established that YREE sorption is strongly influenced by pH. In addition to an increase in the absolute magnitude of YREE sorption with increasing pH, Bau (1999) showed that there is a pH dependence in the pattern of YREE fractionation. Based on experimental results from Eu and La sorption onto hematite, Rabung et al. (1998a) and Marmier and Fromage (1999) used a surface complexation model to describe sorption intensity as a function of pH. Extending the work of Rabung et al. (1998a) and Marmier and Fromage (1999) to include the entire YREE series, Quinn et al. (2006) modeled YREE distribution coefficient results ($3.9 \leqslant pH \leqslant 7.1$) in terms of free ion ($M^{3+}$) sorption with a two-site surface complexation model.

Relatively few studies have compared YREE sorption in the absence and presence of solution complexation. Fairhurst et al. (1995) and Rabung et al. (1998b) showed that Eu^{3+} sorption onto hematite was suppressed at $pH > 5.0$ in the presence of humic acid and fulvic acid. At lower pH values, Eu^{3+} sorption was enhanced to varying degrees, depending on the concentration of humic acid (Fairhurst et al., 1995). Davranche et al. (2004) studied sorption of the entire REE series onto iron oxyhydroxide. A flat YREE sorption pattern was observed in the presence of humic acid, compared to an HREE-enriched pattern in the absence of solution complexation (Davranche et al., 2004). YREE sorption in these studies was interpreted in terms of complexation with humate, with the latter being both dissolved in solution and sorbed onto hematite (Fairhurst et al., 1995; Rabung et al., 1998b; Davranche et al., 2004).

Despite the fact that YREE solution complexation in the open ocean appears to be dominated by carbonate ions (Byrne and Sholkovitz, 1996), its direct role in YREE sorption is poorly understood. Koeppenkastrop and De Carlo (1993) observed that carbonate complexation slowed the rate of uptake of Eu by manganese and iron oxides. Based on their observations of sorption kinetics, Koeppenkastrop and De Carlo (1993) proposed that dissolved REEs dissociate from carbonate ligands before being sorbed as free ions onto a solid. Kawabe et al. (1999b) and Ohta and Kawabe (2000) investigated YREE sorption onto amorphous ferric hydroxide in the presence of carbonate over a narrow pH range (7.6–8.7) at an ionic strength of ~0.5 M. Their results showed that HREE sorption was strongly suppressed in the presence of strong carbonate complexation. Despite the fact that YREE solution chemistry is relatively well understood compared to YREE surface chemistry, Ohta and Kawabe (2000) used their distribution coefficient results along with a theoretical model of surface complexation to derive YREE-carbonate solution complexation constants. As discussed by Luo and Byrne (2004), the results obtained by Ohta and Kawabe (2000) are approximately an order of magnitude larger than previous results obtained using a variety of procedures: solubility (e.g., Ferri et al., 1983), solvent exchange (e.g., Liu and Byrne, 1998), and potentiometry (e.g., Luo and Byrne, 2004).

In the present study, we have examined the effect of carbonate solution complexation on YREE sorption by amorphous ferric hydroxide at low ionic strength ($I < 0.1$ M) over a relatively wide range of pH (4.0–7.1). Distribution coefficient results are quantitatively examined using the surface complexation model of Quinn et al. (2006) and the carbonate complexation constants of Luo and Byrne (2004). Experimental results are used to extend the model of Quinn et al. (2006) to include sorption of YREE solution complexes (i.e., (MCO_3^+) in addition to sorption of free YREE ions (M^{3+}).

2. Theory

Measurements of YREE solution concentrations in the presence of freshly precipitated amorphous ferric hydrox-

ide and dissolved carbonate ($0\ M \leqslant [CO_3^{2-}]_T \leqslant 150\mu M$) were used to calculate distribution coefficients (${}_iK^T_{Fe}$) in the following form:

$${}_iK^T_{Fe} = \frac{[MS_i]_T}{M_T[S_i]}, \quad (1)$$

where $[MS_i]_T$ is the total molar concentration of a sorbed YREE, M_T is the total molar concentration of a dissolved YREE, and $[S_i]$ is the total molar concentration of precipitated amorphous ferric hydroxide. The total concentration of a sorbed YREE can be written as the sum of three or more terms. As one example, in solutions containing carbonate, $[MS_i]_T$ can be written as:

$$[MS_i]_T = [S\text{–}FeO(OH)_2M^{2+}] + [S\text{–}FeO_2(OH)M^{+}] + [S\text{–}FeO(OH)_2MCO_3{}^0]. \quad (2)$$

The first two terms on the right-hand side of Eq. (2) follow from the work of Quinn et al. (2006) in carbonate-free solutions. The final term in Eq. (2) is one of a number of potentially important surface-bound YREE species. Equilibrium constants for the formation of $S\text{–}FeO(OH)_2M^{2+}$, $S\text{–}FeO_2(OH)M^{+}$, and $S\text{–}FeO(OH)_2MCO_3{}^0$ can be written, respectively, as:

$${}_s\beta_1 = \frac{[S\text{–}FeO(OH)_2M^{2+}][H^+]}{[M^{3+}][S\text{–}Fe(OH)_3]}, \quad (3)$$

$${}_s\beta_2 = \frac{[S\text{–}FeO_2(OH)M^{+}][H^+]^2}{[M^{3+}][S\text{–}Fe(OH)_3]}, \quad (4)$$

and

$${}^{CO_3}_{S}\beta_1 = \frac{[S\text{–}FeO(OH)_2MCO_3{}^0][H^+]}{[MCO_3^+][S\text{–}Fe(OH)_3]}, \quad (5)$$

where brackets denote concentrations of the indicated species and $S\text{–}Fe(OH)_3$ represents uncharged amorphous ferric hydroxide surface sites (as distinguished from $S\text{–}Fe(OH)_2{}^+$ and $S\text{–}Fe(OH)_4{}^-$. Under the conditions of our experiments, $S\text{–}Fe(OH)_4{}^-$ is unimportant (Quinn et al., 2006) and the concentration of $S\text{–}Fe(OH)_3$ in Eqs. (3)–(5) can be expressed in terms of $[S_i]$ (Eq. (1)) via the equation:

$$[S\text{–}Fe(OH)_3] = [S_i]({}_sK_1[H^+] + 1)^{-1}, \quad (6)$$

where ${}_sK_1$ is the surface protonation constant for amorphous ferric hydroxide:

$${}_sK_1 = \frac{[S\text{–}Fe(OH)_2{}^+]}{[S\text{–}Fe(OH)_3{}^0][H^+]}. \quad (7)$$

The value of ${}_sK_1$ used in this study (i.e., $\log {}_sK_1 = 4.76$) was taken from the work of Quinn et al. (2006).

For carbonate-free solutions (i.e., $[S\text{–}FeO(OH)_2MCO_3{}^0] = 0$ M), Eqs. (1)–(4), (6) and (7) were used by Quinn et al. (2006) to model YREE sorption in the absence of significant solution complexation. In the presence of YREE carbonate complexation, additional sorbed species must be considered in Eq. (2) including the putative species $S\text{–}FeO(OH)_2MCO_3{}^0$ (Eq. (5)). Additionally, the sorption model of Quinn et al. (2006) must be extended to include the relationship between total dissolved YREE concentrations (M_T) and free YREE concentrations ($[M^{3+}]$) as follows:

$$M_T = [M^{3+}] \times (1 + {}_{HCO_3}\beta_1[HCO_3{}^-]_T + {}^{H}_{CO_3}\beta_1[HCO_3{}^-]_T[H^+]^{-1} + {}^{H}_{CO_3}\beta_2[HCO_3{}^-]^2_T[H^+]^{-2}), \quad (8)$$

where the YREE solution complexation constants (${}_{HCO_3}\beta_1$, ${}^{H}_{CO_3}\beta_1$, and ${}^{H}_{CO_3}\beta_2$) are expressed in terms of bicarbonate concentrations (Luo and Byrne, 2004):

$${}_{HCO_3}\beta_1 = \frac{[MHCO_3{}^{2+}]}{[M^{3+}][HCO_3{}^-]_T}, \quad (9)$$

$${}^{H}_{CO_3}\beta_1 = \frac{[MCO_3{}^+][H^+]}{[M^{3+}][HCO_3{}^-]_T}, \quad (10)$$

and

$${}^{H}_{CO_3}\beta_2 = \frac{[M(CO_3)_2^-][H^+]^2}{[M^{3+}][HCO_3{}^-]^2_T}, \quad (11)$$

and $[HCO_3{}^-]_T$ is the sum concentration of free bicarbonate ions ($HCO_3{}^-$) and ion pairs ($NaHCO_3{}^0$). A term for the formation of MOH^{2+} is not included in Eq. (8) since Quinn et al. (2006) showed that, even in the absence of carbonate complexation, the influence of hydrolysis on the behavior of ${}_iK^T_{Fe}$ at $pH \leqslant 7.0$ is insignificant.

Eqs. (1)–(11) can be combined to produce an equilibrium model for YREE sorption by amorphous ferric hydroxide in the presence of carbonate:

$${}_iK^T_{Fe} = \frac{({}_s\beta_1[H^+]^{-1} + {}_s\beta_2[H^+]^{-2} + {}^{CO_3}_{S}\beta_1 \times {}^{H}_{CO_3}\beta_1[HCO_3{}^-]_T[H^+]^{-2})}{({}_sK_1[H^+] + 1) \times (1 + {}_{HCO_3}\beta_1[HCO_3{}^-]_T + {}^{H}_{CO_3}\beta_1[HCO_3{}^-]_T[H^+]^{-1} + {}^{H}_{CO_3}\beta_2[HCO_3{}^-]^2_T[H^+]^{-2})}. \quad (12)$$

Empirical ${}_iK^T_{Fe}$ data, as defined by Eq. (1), were fit using Eq. (12) with the residual sum of squares (RSS) function as follows:

$$RSS = \sum \left\{ 1 - \left[\left(\frac{{}_s\beta_1[H^+]^{-1} + {}_s\beta_2[H^+]^{-2} + {}^{CO_3}_{S}\beta_1 \times {}^{H}_{CO_3}\beta_1[HCO_3{}^-]_T[H^+]^{-2}}{{}_sK_1[H^+] + 1} \right) \times \left(\frac{[M^{3+}]}{M_T} \right) \times \left({}_iK^T_{Fe} \right)^{-1} \right] \right\}^2. \quad (13)$$

Defined in this manner, the RSS provides equal weight to each experimental ${}_iK^{T}_{Fe}$ result as distribution coefficients range over more than five orders of magnitude.

The carbonate complexation constants in Eq. (12) were taken from the results of Luo and Byrne (2004):

$$\log {}_{HCO_3}\beta_1 = \log {}_{HCO_3}\beta_1^0 - 3.066 \times I^{0.5}/(1 + 1.269 \times I^{0.5}) + 0.297 \times I, \quad (14)$$

$$\log {}^{H}_{CO_3}\beta_1 = \log {}^{H}_{CO_3}\beta_1^0 - 4.088 \times I^{0.5}/(1 + 3.033 \times I^{0.5}) + 0.042 \times I, \quad (15)$$

and

$$\log {}^{H}_{CO_3}\beta_2 = \log {}^{H}_{CO_3}\beta_2^0 - 4.088 \times I^{0.5}/(1 + 3.033 \times I^{0.5}) + 0.042 \times I, \quad (16)$$

where the values of $\log {}_{HCO_3}\beta_1^0$, $\log {}^{H}_{CO_3}\beta_1^0$, and $\log {}^{H}_{CO_3}\beta_2^0$ for each YREE can be found in Table 5 of Luo and Byrne (2004). Bicarbonate concentrations were calculated from the equation:

$$[HCO_3^-]_T = K_0K_1'P_{CO_2}[H^+]^{-1}, \quad (17)$$

where the product K_0K_1' describes the equilibrium:

$$CO_2\ (g) + H_2O \rightleftharpoons HCO_3^- + H^+. \quad (18)$$

The CO_2 partial pressure (P_{CO_2}) in Eq. (17) is expressed in terms of the total atmospheric pressure (P_T), the partial pressure of H_2O at 25 °C (P_{H_2O}), and the mole fraction of CO_2/N_2 gas mixtures (X_{CO_2}) using the following equation:

$$P_{CO_2} = X_{CO_2}(P_T - P_{H_2O}) = 0.969X_{CO_2}\ \text{atm}. \quad (19)$$

K_0K_1' data appropriate to Eq. (18) were taken from the results of Luo and Byrne (2004):

$$\log K_0K_1' = -7.829 + 1.022 \times I^{0.5}/(1 + 1.390 \times I^{0.5}) - 0.191 \times I. \quad (20)$$

For the purpose of creating graphs, carbonate concentrations were calculated using the following equation:

$$[CO_3^{2-}]_T = K_0K_1'K_2'P_{CO_2}[H^+]^{-2}, \quad (21)$$

where $[CO_3^{2-}]_T$ is the sum concentration of free carbonate ions (CO_3^{2-}) and ion pairs ($NaCO_3^-$), and K_2' is the equilibrium constant for the dissociation of bicarbonate:

$$HCO_3^- \rightleftharpoons CO_3^{2-} + H^+. \quad (22)$$

K_2' was calculated from the results of Luo and Byrne (2004):

$$\log K_2' = -10.331 + 2.044 \times I^{0.5}/(1 + 1.060 \times I^{0.5}) - 0.184 \times I. \quad (23)$$

Eqs. (14)–(23) explicitly show the substantial ionic strength dependences for equilibria in the solution phase. In contrast, a wide variety of previous work has shown that the affinities of sorptive solid substrates for dissolved cations do not vary with ionic strength (Swallow et al., 1980; Hayes and Leckie, 1987; Dzombak and Morel, 1990; Quinn et al., 2006). The data of Quinn et al. (2006) showed that the influence of ionic strength on ${}_S\beta_1$ and ${}_S\beta_2$ (Eqs. (3) and (4)) was very weak. Based on these observations appropriate to the YREEs, and a variety of observations obtained using other cations (Swallow et al., 1980; Hayes and Leckie, 1987), it was assumed in this work that not only ${}_S\beta_1$ and ${}_S\beta_2$ but also ${}^{CO_3}_{S}\beta_1$ (Eq. (5)) was invariant over the range of ionic strength utilized in this investigation ($0.01\ M \leqslant I \leqslant 0.1\ M$). It should be noted in this case that the product ${}^{CO_3}_{S}\beta_1 \times {}^{H}_{CO_3}\beta_1$ has an ionic strength dependence identical to that of ${}^{H}_{CO_3}\beta_1$ (Eq. (15)).

3. Materials and methods

Three types of experiment were undertaken to investigate the influence of carbonate solution complexation on YREE sorption by amorphous ferric hydroxide. In one type of experiment, sorption was examined as a function of time at constant pH and constant P_{CO_2}. In the other types of experiment, either solution pH was increased at constant P_{CO_2} or the P_{CO_2} was increased at constant pH.

All solutions were prepared with trace metal clean water (Milli-Q water) from a Millipore (Bedford, MA) purification system. Ammonium nitrate (99.999%) and certified 1.000 M hydrochloric acid were purchased from Sigma–Aldrich (St. Louis, MO). TraceMetal Grade nitric acid, TraceMetal Grade ammonium hydroxide, and ferric chloride solution (40% w/v in HCl) were purchased from Fisher Scientific (Pittsburgh, PA). Sodium bicarbonate (Baker analyzed) was purchased from J.T. Baker Inc. (Phillipsburg, NJ). A YREE stock solution, containing 66.7 ppm of each YREE in 2% HNO_3, was prepared from single-element ICP standards (SPEX CertiPrep, Metuchen, NJ). Ultra-pure N_2 and various certified CO_2/N_2 gas mixtures (30%, 3%, 1%, 0.5%, 0.3%, 0.1%, and 0.01% CO_2) were obtained from Airgas South Inc. (Clearwater, FL).

All chemical manipulations were performed in a class-100 clean air laboratory or laminar flow bench. Teflon and polypropylene laboratory materials and polycarbonate filter membranes were cleaned by soaking in HCl or HNO_3 for at least a week, followed by several thorough rinses with Milli-Q water. Solution pH, on the free hydrogen ion scale, was monitored using a Ross-type combination pH electrode (No. 810200) connected to a Corning 130 pH meter in the absolute millivolt mode. Nernstian behavior of the electrode was verified periodically by titrating a 0.3 M NaCl solution with concentrated HCl.

At the beginning of each experiment, a pH standard solution and an experimental solution, both with an ionic strength (I) equal to 0.011 M, were prepared in Teflon wide-mouth bottles. The pH standard solution was composed of 1 mM HCl (pH 3.0) in 0.01 M NH_4NO_3. The experimental solution was composed of 107.8 μM ferric iron and 23.3 ppb of each YREE ($[YREE]_T = 2.36\ \mu M$) in 0.01 M HCl. Both solutions were placed in jacketed beakers thermostated at $T = (25.0 \pm 0.1)$ °C and were

equilibrated for approximately 24 h. Throughout each experiment, solutions were continuously stirred with a Teflon-coated 'floating' stir bar and the experimental solution was continuously bubbled with a gas mixture, except during titrant additions. Ultra-pure N_2 gas was first passed through an in-line trap (Supelco, Bellafonte, PA) that removed all traces of CO_2. After bubbling for 1 h at pH 2.0, starting with ultra-pure N_2 for experiments conducted over a range of P_{CO_2}, and with either 3% or 30% CO_2 for experiments at constant P_{CO_2}, an initial solution sample was taken to determine the total dissolved YREE concentration, M_T. Solution pH was then increased by addition of 0.7 M $NaHCO_3$ with a Gilmont micro-dispenser, resulting in rapid formation of a yellow-brown $Fe(OH)_3$ colloid.

One experiment was performed at constant P_{CO_2} (30%) and constant pH (5.4), and samples were taken at 15 min, 90 min, 5 h, 24 h, 46 h, and 48 h. Two experiments were performed at constant P_{CO_2} and increasing pH: one at 3% CO_2 and the other at 30% CO_2. Samples were taken at fixed pH increments between 4.0 and 6.6 after the solution had been equilibrated with the gas mixture for 1 h. Four experiments were performed at increasing P_{CO_2} and constant pH: two at pH $\sim$ 6.6 and two at pH $\sim$ 7.1. After taking the initial sample (pH 2.0), the pH was raised by addition of 1 M NH_4OH using a Gilmont micro-dispenser. While bubbling with ultra-pure N_2, four samples were taken: one at 15 min, one at 90 min, one at 5 h, and one at $\sim$22 h. Subsequently, CO_2/N_2 gas mixtures were used to progressively increase P_{CO_2} between 0.01% and 30% CO_2 (two experiments) and between 0.3% and 30% CO_2 (two experiments). After each P_{CO_2} increase, solutions were equilibrated for approximately 1 h. The pH was then readjusted by addition of 1 M $NaHCO_3$. At each P_{CO_2}, samples were taken at 15 min, 90 min, and either $\sim$22 h or between 45 and 70 h. Occasionally, a fourth sample was taken at 47 or 66 h. Because increases in the carbonate concentration caused increases in the ionic strength of the experimental solutions, the ionic strengths of pH standard solutions were matched using 1 M NH_4NO_3.

The sampling method was similar to that described in Quinn et al. (2006). To summarize, during most experiments two samples were collected, one filtered and one centrifuged. During a few experiments, only filtered samples were taken because better phase separation was achieved with filtration. Each filtered sample consisted of two 5-mL aliquots of solution. The first was used to rinse the polypropylene syringe and the Nuclepore filter membrane (polycarbonate, 0.10 μm pore size). The second was collected in a polypropylene centrifuge tube. The centrifuged sample consisted of one 5-mL aliquot of solution, which was centrifuged for 1 h using a Centra-4B centrifuge (International Equipment Company, Needham Heights, MA) at about 2200*g*.

The filtered samples and the supernatant of the centrifuged samples were diluted fivefold with 1% HNO_3 except where concentrations were below the lowest calibration standard (0.5 ppb), in which case no dilution was performed. A small amount of internal standard solution containing equal concentrations of In, Cs, and Re was added to each sample. The resulting mixtures were analyzed for YREEs with an Agilent Technologies 4500 Series 200 inductively-coupled plasma mass spectrometer (ICP-MS) following the procedure outlined in Quinn et al. (2004). In brief, all standards and sample solutions were injected in triplicate. During instrument tuning, the formation of oxide and double-charged ions was minimized with a 10 ppb Ce solution. MO^+ and M^{2+} peaks were always less than 1% and 3% of the corresponding M^+ peak, respectively, and correction for this effect proved unnecessary. YREE concentrations were calculated from linear regressions of four standards (0.5, 1, 2, and 5 ppb). Ion counts were corrected for minor instrument drift by normalizing ^{89}Y to ^{115}In, ^{139}La –^{161}Dy to ^{133}Cs, and ^{163}Dy –^{175}Lu to ^{187}Re. To check the validity of the drift correction, a comparison was made of the Dy concentrations calculated from ^{161}Dy and ^{163}Dy, which were usually identical within 2%.

For each experiment, raw ICP-MS data were corrected for dilution based on the volume of NH_4OH and/or $NaHCO_3$ titrants added to adjust the pH. Corrected data were then used to calculate distribution coefficients ($_iK_{Fe}^T$) defined by Eq. (1). The concentration of sorbed YREE, $[MS_i]_T$, was calculated as the difference between the YREE concentration in the initial sample (pH 2.0) and the YREE concentrations in subsequent samples after a pH or P_{CO_2} adjustment. Based on the solubility behavior of Fe^{3+} (Liu and Millero, 1999), the concentration of precipitated iron at pH > 4.0 was assumed to be equal to the initial dissolved iron concentration ($\sim$100 μM).

Quinn et al. (2006) noted that YREE equilibrium between experimental solutions and freshly precipitated $Fe(OH)_3$ is reached in about 15 min. In the present work, variations in $\log {}_iK_{Fe}^T$ for equilibration times $\geqslant$15 min are smaller than the uncertainty in experimental $\log {}_iK_{Fe}^T$ values. Therefore all data in Appendix A, which lists 111 $\log {}_iK_{Fe}^T$ observations for each rare earth element, were used in our data analysis, except for two observations identified in Table A.3. These were obtained under conditions (pH 3.98 and pH 4.49) that produced very weak sorption, and therefore poorly constrained $\log {}_iK_{Fe}^T$ data. This problem was expected, a priori, from the work of Quinn et al. (2006), in which well defined $\log {}_iK_{Fe}^T$ results at low pH ($\sim$4.0) were obtained by conducting experiments using 10 mM concentrations of precipitated amorphous ferric hydroxide. Utilization of the data of Quinn et al. (2006) (their Tables A.1–A.6) along with the data shown in Appendix A resulted in regressions via Eqs. (12) and (13) that incorporated as many as 166 $\log {}_iK_{Fe}^T$ observations for each REE.

4. Results and discussion

4.1. Model results considering sorption of only free YREEs

Since carbonate-free samples were included in the present experiments, $_S\beta_1$ and $_S\beta_2$ values were recalculated using

new non-carbonate ${}_iK^{T}_{Fe}$ data (Tables A4–A7) plus the previous non-carbonate ${}_iK^{T}_{Fe}$ data of Quinn et al. (2006) (their Tables A.1–A.6). The ${}_S\beta_1$ and ${}_S\beta_2$ results calculated using Eqs. (12) and (13) with $[HCO_3^-]_T = 0$ M are listed in Table 1. Comparison of these results with the ${}_S\beta_1$ and ${}_S\beta_2$ results of Quinn et al. (2006) demonstrates agreement within approximately 1%, well within the listed uncertainties for both constants.

Distribution coefficient results from experiments containing carbonate were initially modeled by assuming that only free YREE ions sorb onto amorphous ferric hydroxide. In this case, the ${}^{CO_3}_S\beta_1$ term in Eq. (12) is zero. Fig. 1A shows $\log {}_iK^{T}_{Fe}$ patterns at pH 7.06 predicted using Eq. (12) with the ${}_S\beta_1$ and ${}_S\beta_2$ results listed in Table 1 and ${}^{CO_3}_S\beta_1 = 0$. Predicted $\log {}_iK^{T}_{Fe}$ values decrease monotonically with increasing $[CO_3^{2-}]_T$, and the decrease in $\log {}_iK^{T}_{Fe}$ for heavy REEs is approximately four orders of magnitude.

Fig. 1B shows experimental $\log {}_iK^{T}_{Fe}$ results obtained at pH 7.06 for the same carbonate concentrations depicted in Fig. 1A. In sharp contrast to the predicted behavior shown in Fig. 1A, measured $\log {}_iK^{T}_{Fe}$ values at low carbonate concentrations are larger than those at $[CO_3^{2-}]_T = 0$ M. Furthermore, the range of $\log {}_iK^{T}_{Fe}$ values shown in Fig. 1B is orders of magnitude smaller than the predictions shown in Fig. 1A. Predicted and observed $\log {}_iK^{T}_{Fe}$ values are directly and quantitatively compared in Fig. 2. In the absence of carbonate (open circles), $\log {}_iK^{T}_{Fe}$ values are well described using Eq. (12). In the presence of carbonate (closed circles), $\log {}_iK^{T}_{Fe}$ observations are uniformly larger than Eq. (12) $\log {}_iK^{T}_{Fe}$ predictions obtained assuming ${}^{CO_3}_S\beta_1 = 0$. Fig. 2 clearly shows that YREE sorption data in the presence of carbonate cannot be appropriately modeled solely in terms of the sorption of free ions, M^{3+}.

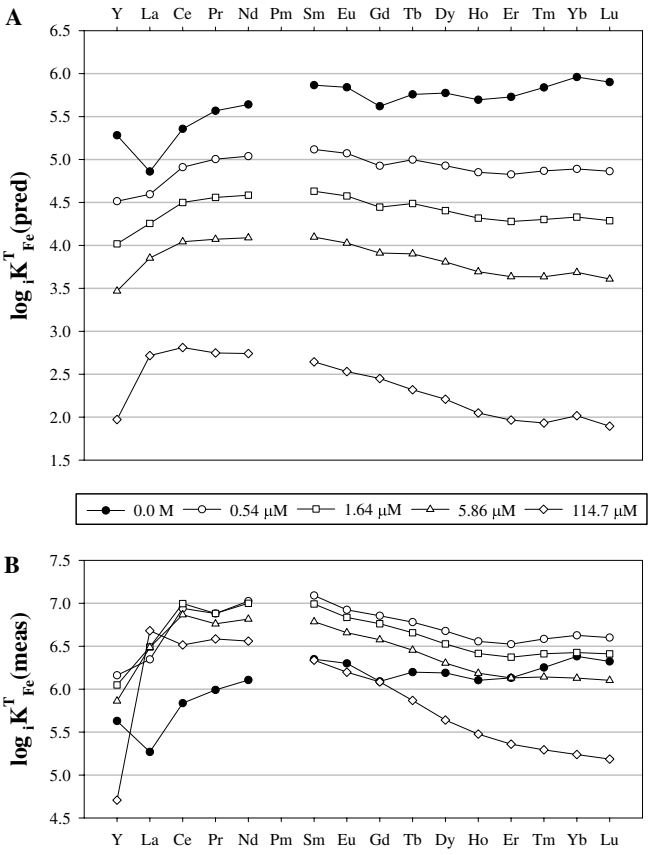

Fig. 1. $\log {}_iK^{T}_{Fe}$ results at pH 7.06 and various carbonate concentrations, $[CO_3^{2-}]_T$, listed in the legend. (A) $\log {}_iK^{T}_{Fe}$(pred) are distribution coefficients predicted from Eq. (12) using the ${}_S\beta_1$ and ${}_S\beta_2$ results listed in Table 1 and ${}^{CO_3}_S\beta_1 = 0$. (B) $\log {}_iK^{T}_{Fe}$(meas) are directly measured distribution coefficients from an experiment performed at constant pH (7.06) and increasing P_{CO_2} (Table A.6). Each pattern represents an average over time for a single carbonate concentration. For clarity, the $\log {}_iK^{T}_{Fe}$ pattern at $[CO_3^{2-}]_T = 0.88$ μM ($P_{CO_2} = 0.5\%$) is not shown.

Table 1
YREE surface complexation constants (${}_S\beta_1$ and ${}_S\beta_2$) determined using Eqs. (12) and (13) with $[HCO_3^-]_T = 0$ M, $\log {}_SK_1 = 4.76$ (Quinn et al., 2006), the experimental distribution coefficient results from Quinn et al. (2006) (their Tables A.1–A.6), and the experimental ${}_iK^{T}_{Fe}$ results from carbonate-free solutions in the present work (Tables A4–A7)

$[M^{3+}]$	$\log {}_S\beta_1$	$\log {}_S\beta_2$
Y	−2.98 ± 0.06	−8.86 ± 0.05
La	−2.87 ± 0.04	−9.36 ± 0.07
Ce	−2.38 ± 0.04	−8.86 ± 0.08
Pr	−2.26 ± 0.04	−8.63 ± 0.06
Nd	−2.18 ± 0.04	−8.55 ± 0.07
Pm	—	—
Sm	−2.06 ± 0.04	−8.31 ± 0.06
Eu	−2.11 ± 0.04	−8.33 ± 0.05
Gd	−2.28 ± 0.04	−8.56 ± 0.06
Tb	−2.29 ± 0.04	−8.40 ± 0.05
Dy	−2.32 ± 0.03	−8.38 ± 0.04
Ho	−2.37 ± 0.03	−8.46 ± 0.05
Er	−2.33 ± 0.03	−8.43 ± 0.05
Tm	−2.24 ± 0.03	−8.32 ± 0.04
Yb	−2.17 ± 0.03	−8.19 ± 0.04
Lu	−2.17 ± 0.03	−8.26 ± 0.05

Uncertainties represent one standard error.

4.2. Model results including sorption of a YREE carbonate complex

Non-linear least squares regressions (Eqs. (12) and (13)) of the combined (carbonate plus non-carbonate) $\log {}_iK^{T}_{Fe}$ data obtained in this work and in Quinn et al. (2006) produced well-constrained estimates for ${}^{CO_3}_S\beta_1$ as well as ${}_S\beta_1$ and ${}_S\beta_2$ (Table 2). Figs. 3A, B, and C provide graphical representations of the ${}_S\beta_1$, ${}_S\beta_2$, and ${}^{CO_3}_S\beta_1$ data given in Table 2 (open circles). Also shown in Fig. 3A and Fig. 3B are the ${}_S\beta_1$ and ${}_S\beta_2$ data given in Table 1 (closed circles). The ${}^{CO_3}_S\beta_1$ results in Fig. 3C (closed circles) were obtained in fits (Eqs. (12) and (13)) of data at $[CO_3^{2-}]_T > 0$ M using the ${}_S\beta_1$ and ${}_S\beta_2$ values from Table 1. It is seen in Fig. 3A and Fig. 3B that $\log {}_S\beta_1$ and $\log {}_S\beta_2$ results obtained in both two-parameter fits (${}_S\beta_1$ and ${}_S\beta_2$ in Table 1) and three-parameter fits (${}_S\beta_1$, ${}_S\beta_2$, and ${}^{CO_3}_S\beta_1$ in Table 2) are in very good agreement. Fig. 3C shows that $\log {}^{CO_3}_S\beta_1$ results from three-parameter fits (${}_S\beta_1$, ${}_S\beta_2$, and ${}^{CO_3}_S\beta_1$ in Table 2) and from single-parameter fits (${}_S\beta_1$ and ${}_S\beta_2$ taken from Table 1) are indistinguishable. The pattern in Fig. 3D, which represents

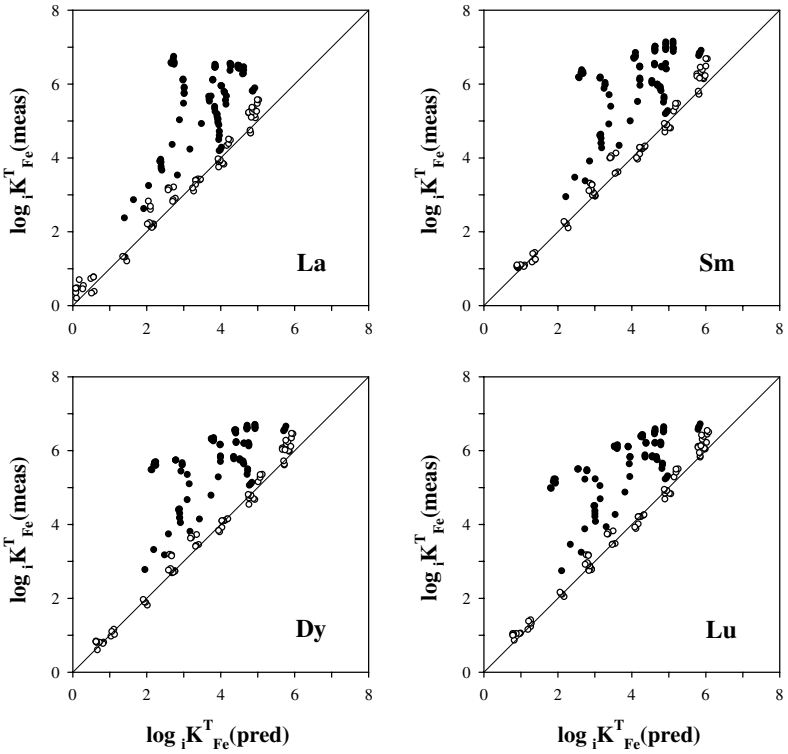

Fig. 2. $\log {}_iK^{T}_{Fe}$(meas) versus $\log {}_iK^{T}_{Fe}$(pred) for La, Sm, Dy, and Lu. $\log {}_iK^{T}_{Fe}$(meas) are directly measured distribution coefficients from the present work (Tables A1–A7) and from Quinn et al. (2006) (their Tables A.1–A.6). Observed $\log {}_iK^{T}_{Fe}$ values represent YREE sorption corresponding to 5.0 – 99.9% of the total YREE concentration. $\log {}_iK^{T}_{Fe}$(pred) are distribution coefficients predicted from Eq. (12) using the $_S\beta_1$ and $_S\beta_2$ results listed in Table 1 and $^{CO_3}_{S}\beta_1 = 0$. Open circles represent carbonate-free samples and closed circles represent samples containing carbonate. Diagonal lines represent perfect agreement between predicted and measured values ($\log {}_iK^{T}_{Fe}$(pred) = $\log {}_iK^{T}_{Fe}$(meas)).

Table 2
YREE surface complexation constants ($_S\beta_1$, $_S\beta_2$, and $^{CO_3}_{S}\beta_1$) determined with Eqs. (12) and (13), $\log {}_SK_1 = 4.76$ (Quinn et al., 2006), the experimental distribution coefficient results from Quinn et al. (2006) (their Tables A.1–A.6), and the experimental $_iK^{T}_{Fe}$ results from the present work (Tables A1–A7)

[M^{3+}]	$\log {}_S\beta_1$	$\log {}_S\beta_2$	$\log {}^{CO_3}_{S}\beta_1$
Y	−2.98 ± 0.07	−8.82 ± 0.05	−1.30 ± 0.04
La	−2.86 ± 0.03	−9.34 ± 0.06	−0.39 ± 0.02
Ce	−2.38 ± 0.04	−8.84 ± 0.07	−0.21 ± 0.02
Pr	−2.25 ± 0.03	−8.60 ± 0.06	−0.22 ± 0.02
Nd	−2.17 ± 0.04	−8.53 ± 0.06	−0.20 ± 0.02
Pm	—	—	—
Sm	−2.05 ± 0.04	−8.29 ± 0.05	−0.20 ± 0.02
Eu	−2.11 ± 0.04	−8.31 ± 0.05	−0.26 ± 0.02
Gd	−2.28 ± 0.03	−8.54 ± 0.05	−0.38 ± 0.02
Tb	−2.29 ± 0.03	−8.38 ± 0.04	−0.40 ± 0.02
Dy	−2.32 ± 0.03	−8.36 ± 0.04	−0.51 ± 0.02
Ho	−2.36 ± 0.03	−8.44 ± 0.04	−0.57 ± 0.02
Er	−2.33 ± 0.03	−8.40 ± 0.04	−0.59 ± 0.02
Tm	−2.24 ± 0.03	−8.29 ± 0.04	−0.56 ± 0.02
Yb	−2.17 ± 0.04	−8.16 ± 0.04	−0.62 ± 0.02
Lu	−2.17 ± 0.03	−8.23 ± 0.04	−0.59 ± 0.02

Uncertainties represent one standard error.

the product $^{CO_3}_{S}\beta_1 \times {}^{H}_{CO_3}\beta_1$ used in Eq. (12), was obtained by multiplying the formation constant for the surface species S–FeO(OH)$_2$MCO_3^0 ($^{CO_3}_{S}\beta_1$; Table 2) and the formation constant for the solution species MCO_3^+ at zero ionic strength ($^{H}_{CO_3}\beta^0_1$; taken from Luo and Byrne, 2004). It should be noted that the pattern for $^{CO_3}_{S}\beta_1 \times {}^{H}_{CO_3}\beta_1$ will not change as a function of ionic strength but the absolute magnitude has an ionic strength dependence identical to that of $^{H}_{CO_3}\beta_1$ (Eq. (15)).

As a visual demonstration of the goodness-of-fit for the model, Fig. 4 compares observed $\log {}_iK^{T}_{Fe}$ data in the absence (open circles) and presence (closed circles) of carbonate with $\log {}_iK^{T}_{Fe}$ data predicted using Eq. (12) and the parameters given in Table 2. The four REE shown in Fig. 4 are representative of the entire YREE series, which all display excellent fits with slopes close to one and intercepts close to zero. It can be seen that YREE sorption by amorphous ferric hydroxide in the presence of carbonate is well-described by accounting for solution complexation ($MHCO_3^{2+}$, MCO_3^+, and $M(CO_3)_2^-$ formation), and the formation of three surface-bound YREE species (S–FeO(OH)$_2M^{2+}$, S–FeO_2(OH)M^+, and S–FeO(OH)$_2$ MCO_3^0).

In addition to predicted versus observed $\log {}_iK^{T}_{Fe}$ comparisons for individual YREEs, it is also informative to examine predicted versus observed patterns for the entire YREE series. In Fig. 5, directly measured $\log {}_iK^{T}_{Fe}$ patterns are compared with $\log {}_iK^{T}_{Fe}$ patterns predicted from Eq. (12) using the $_S\beta_1$, $_S\beta_2$, and $^{CO_3}_{S}\beta_1$ results listed in Table 2. The $\log {}_iK^{T}_{Fe}$ patterns shown in Fig. 5 were selected from

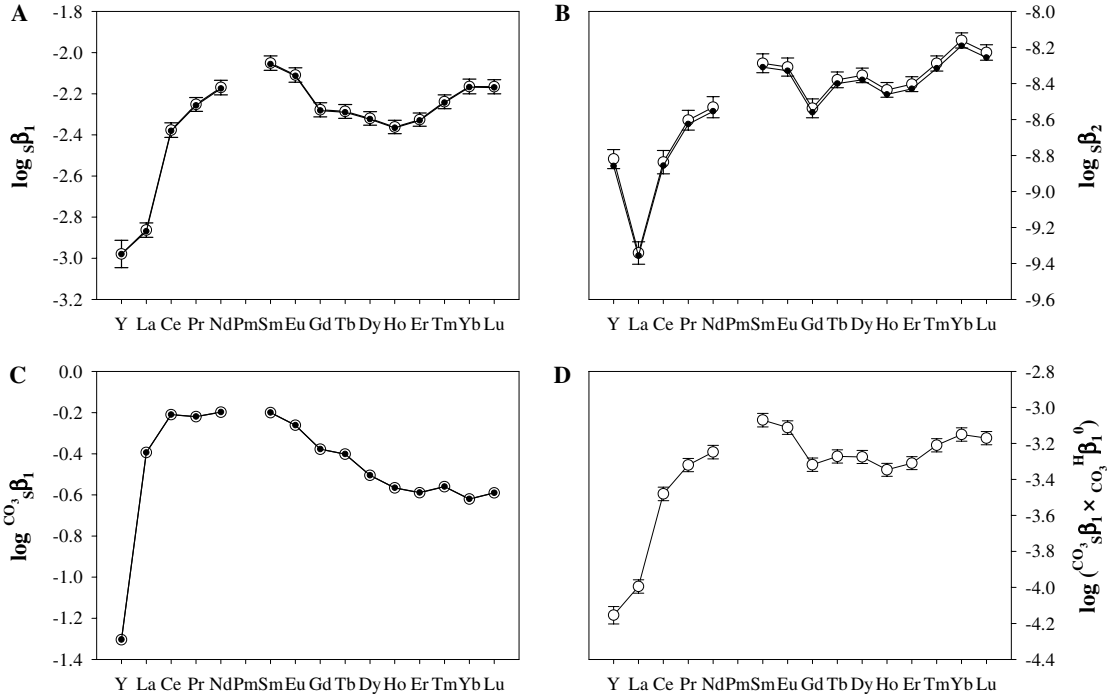

Fig. 3. Surface stability constants (Eq. (12)) for YREE sorption by amorphous ferric hydroxide. Open circles in panels (A), (B), and (C) represent the $_S\beta_1$, $_S\beta_2$, and $^{CO_3}_S\beta_1$ results (Table 2) obtained in three-parameter fits using Eqs. (12) and (13). Open circles in panel (D) represent the product $^{CO_3}_S\beta_1 \times {}^{H}_{CO_3}\beta_1^0$ obtained by multiplying the $^{CO_3}_S\beta_1$ results from the present work and the $^{H}_{CO_3}\beta_1^0$ results from Luo and Byrne (2004). Closed circles in panels (A) and (B) represent the $_S\beta_1$ and $_S\beta_2$ results (Table 1) obtained in two-parameter fits using Eqs. (12) and (13) with $[HCO_3^-]_T = 0\,M$. Closed circles in panel (C) represent the $^{CO_3}_S\beta_1$ results obtained in single-parameter fits using Eqs. (12) and (13). See text for details. Error bars on the open circles represent standard errors. For $^{CO_3}_S\beta_1$, standard errors are within the size of the symbol. For $^{CO_3}_S\beta_1 \times {}^{H}_{CO_3}\beta_1^0$, error bars were determined by statistically combining the standard errors from both stability constants.

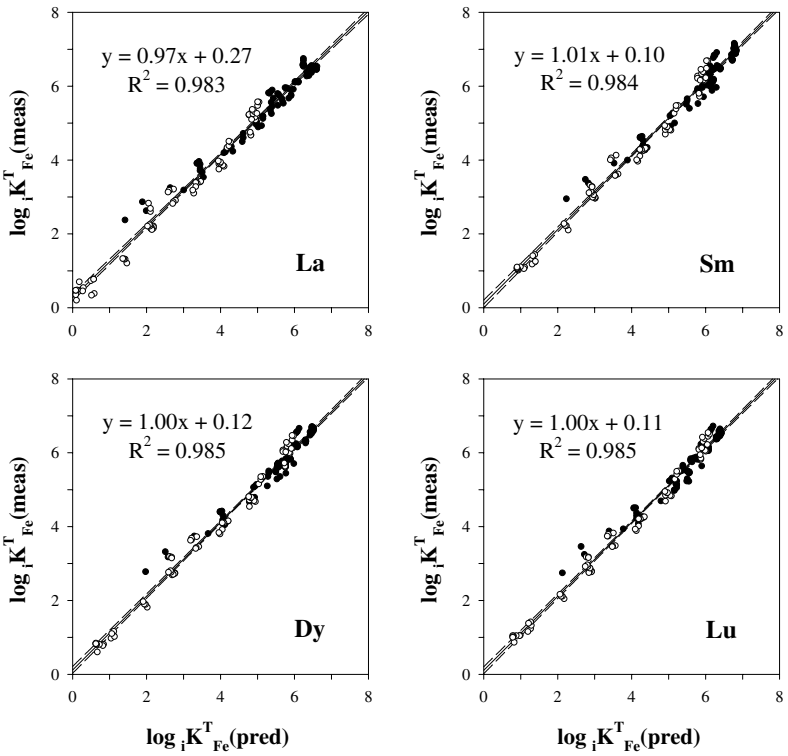

Fig. 4. Regressions of $\log {}_iK^T_{Fe}$(meas) versus $\log {}_iK^T_{Fe}$(pred) for La, Sm, Dy, and Lu. $\log {}_iK^T_{Fe}$(meas) are directly measured distribution coefficients from the present work (Tables A1–A7) and from Quinn et al. (2006) (their Tables A.1–A.6). $\log {}_iK^T_{Fe}$(pred) are distribution coefficients predicted from Eq. (12) using the $_S\beta_1$, $_S\beta_2$, and $^{CO_3}_S\beta_1$ results listed in Table 2. Open circles represent carbonate-free samples and closed circles represent samples containing carbonate. Dashed lines represent 95% confidence intervals.

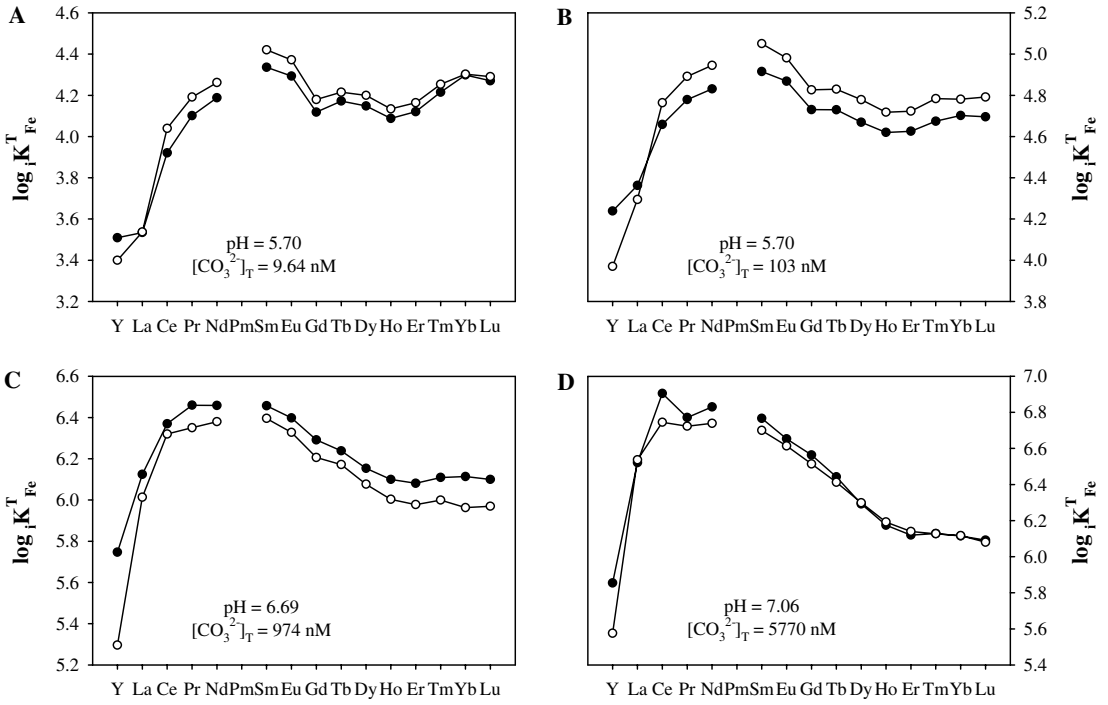

Fig. 5. log $_iK^T_{Fe}$ patterns covering a range of carbonate concentrations. Closed circles represent distribution coefficients experimentally observed in the present work (Tables A2, A3, and A5, A6). Open circles represent distribution coefficients predicted from Eq. (12) using the $_S\beta_1$, $_S\beta_2$, and $^{CO_3}_S\beta_1$ results listed in Table 2.

Appendix A to represent the progression of shapes observed over the range of carbonate concentrations used here. It can be seen that these shapes are generally well predicted using Eq. (12) and the data given in Table 2. Although positive and negative deviations between predicted and measured values are seen in Fig. 5, no systematic differences were observed for the log $_iK^T_{Fe}$ patterns obtained in this investigation.

Other than the species S–FeO(OH)$_2$MCO$_3^0$, two additional terms (S–FeO(OH)$_2$MHCO$_3^+$ and S–FeO$_2$(OH)MCO$_3^-$) were considered in the Eq. (2) summation for [MS$_i$]$_T$. The surface complexation constants for these two species can be written as:

$$^{HCO_3}_S\beta_1 = \frac{[\text{S–FeO(OH)}_2\text{MHCO}_3^+][\text{H}^+]}{[\text{MHCO}_3^{2+}][\text{S–Fe(OH)}_3]}, \quad (24)$$

and

$$^{CO_3}_S\beta_2 = \frac{[\text{S–FeO}_2\text{(OH)MCO}_3^-][\text{H}^+]^2}{[\text{MCO}_3^+][\text{S– Fe(OH)}_3]}. \quad (25)$$

Replacement of the term for S–FeO(OH)$_2$MCO$_3^0$ formation (Eq. (5)) in Eq. (12) with terms for either S–FeO(OH)$_2$MHCO$_3^+$ or S–FeO$_2$(OH)MCO$_3^-$ formation (Eqs. 24 and 25) produced residual sum of squares (RSS) results much inferior to those obtained using Eq. (13). Furthermore, inclusion of terms for S–FeO(OH)$_2$MHCO$_3^+$ and S–FeO$_2$(OH)MCO$_3^-$ in addition to the term for S–FeO(OH)$_2$MCO$_3^0$ led to insubstantial improvements relative to fits with only three surface terms ($_S\beta_1$, $_S\beta_2$, and $^{CO_3}_S\beta_1$). Eq. (12) provides a robust description of the data obtained in this investigation.

Additional sorption terms may be required at higher pH and higher carbonate concentrations than were investigated in the present work. Tang and Johannesson (2005) reported M(CO$_3$)$_2^-$ sorption on Carrizo sand for pH > 7.3. Under the conditions of our experiments (pH ⩽ 7.15), sorption of M(CO$_3$)$_2^-$ was not required to describe partitioning of YREEs between the aqueous phase and amorphous ferric hydroxide.

4.3. Examination of the competing influences of surface and solution complexation on $_iK^T_{Fe}$

The distribution coefficients predicted from Eq. (12) can be separated into contributions from solution species (MHCO$_3^{2+}$, MCO$_3^+$, and M(CO$_3$)$_2^-$) and surface species (S–FeO(OH)$_2$M^{2+}, S–FeO$_2$(OH)M$^+$, and S–FeO(OH)$_2$MCO$_3^0$). This is shown by rearranging Eq. (1) as follows:

$$\log {}_iK^T_{Fe} = \log \frac{[\text{MS}_i]_T}{[\text{M}^{3+}][\text{S}_i]} - \log \frac{\text{M}_T}{[\text{M}^{3+}]}. \quad (26)$$

The first term on the right-hand side of Eq. (26) describes the affinity of amorphous ferric hydroxide for free dissolved YREE ions (M^{3+}). Using Eqs. (2)–(6) and (10), this term is written as:

$$\frac{[MS_i]_T}{[M^{3+}][S_i]} = \frac{{}_S\beta_1[H^+]^{-1} + {}_S\beta_2[H^+]^{-2} + {}^{CO_3}_{S}\beta_1 \times {}^{H}_{CO_3}\beta_1[HCO_3^-]_T[H^+]^{-2}}{{}_SK_1[H^+] + 1}. \quad (27)$$

The second term in Eq. (26) is the complexation intensity of YREEs in solution (i.e., Eq. (8)). This term is a measure of the relative proportions of YREEs that remain in solution as free ions. The competitive influences of surface versus solution complexation on observed $\log {}_iK^T_{Fe}$ patterns (Fig. 5) are shown in Figs. 6 and 7, respectively.

The patterns shown in Fig. 6, which are calculated with Eq. (27), are relatively constant over a wide range of conditions. The uniformity of these patterns is due to the fact that the terms ${}_S\beta_1$, ${}_S\beta_2$, and ${}^{CO_3}_{S}\beta_1 \times {}^{H}_{CO_3}\beta_1$ in Eq. (27) have very similar patterns (Fig. 3A, B, and D) across the YREE series. In contrast, the patterns of the solution complexation term ($M_T/[M^{3+}]$) shown in Fig. 7 exhibit large changes over the same range of conditions.

Eq. (26) indicates that the predicted $\log {}_iK^T_{Fe}$ patterns in Fig. 5 can be obtained by subtracting the solution complexation curves in Fig. 7 from the corresponding surface complexation curves in Fig. 6. Since the solution complexation term labeled A in Fig. 7 is very close to zero and displays a relatively flat pattern, the conjugate $\log {}_iK^T_{Fe}$ pattern at $[CO_3^{2-}]_T = 9.64$ nM (Fig. 5A) closely resembles the pattern for the surface complexation term in Fig. 6A. The $\log {}_iK^T_{Fe}$ values in Fig. 5B are 0.5 to 0.6 units larger than the $\log {}_iK^T_{Fe}$ values shown in Fig. 5A. This is caused by a nearly one unit increase in the magnitude of the surface complexation term (Fig. 6B) and a much smaller increase in the solution complexation intensity (Fig. 7B). Compared to the pattern in Fig. 5A, the $\log {}_iK^T_{Fe}$ pattern at $[CO_3^{2-}]_T = 103$ nM (Fig. 5B) shows a small decrease in the HREEs (e.g., Lu) relative to the middle REEs (e.g., Sm). This is caused by larger increases in HREE solution complexation intensity than is the case for LREEs. The $\log {}_iK^T_{Fe}$ pattern at $[CO_3^{2-}]_T = 974$ nM (Fig. 5C) displays a gradual decrease along the YREE series from Sm to Lu compared to the patterns in Fig. 5A and Fig. 5B. This is due to the rapidly increasing significance in solution complexation for HREEs (Fig. 7C). The $\log {}_iK^T_{Fe}$ pattern at $[CO_3^{2-}]_T = 5770$ nM (Fig. 5D) exhibits a pronounced decrease across the YREE series from Sm to Lu due to the sharp increase in the solution complexation term (Fig. 7D). Although the

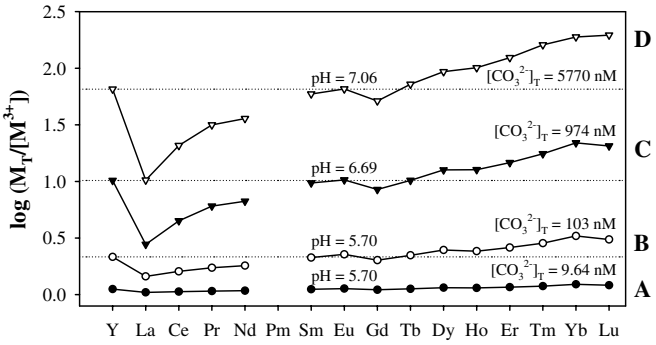

Fig. 7. Patterns of the solution complexation term (log ($M_T/[M^{3+}]$)) in Eq. (26) calculated with Eq. (8). The symbols for each pattern correspond to the same symbols in Fig. 6. Horizontal dotted lines were drawn through Y to emphasize the different slopes of the patterns, except for the pattern at $[CO_3^{2-}]_T = 9.64$ nM, which is relatively flat. For clarity, the vertical axis is extended below zero although all of the solution complexation values are positive.

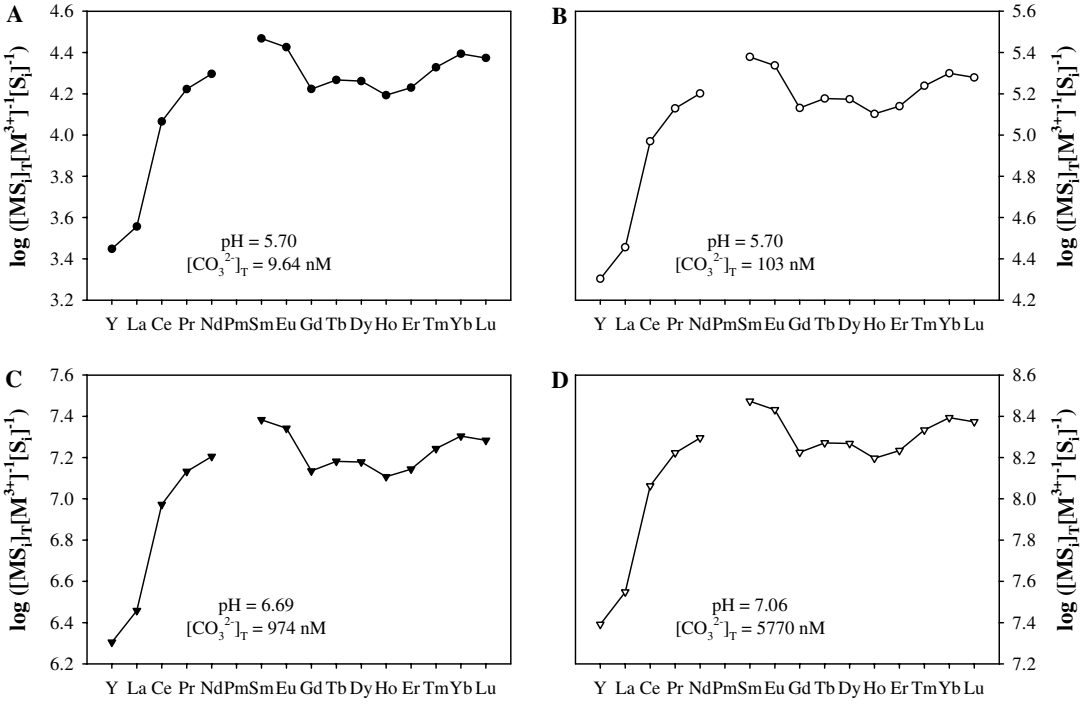

Fig. 6. Patterns of the surface complexation term (log ($[MS_i]_T[M^{3+}]^{-1}[S_i]^{-1}$)) in Eq. (26) calculated with Eq. (27).

magnitudes of $\log {}_iK^{T}_{Fe}$ values increase for all YREEs between Fig. 5A and Fig. 5D, changes are smallest for the HREEs due to the stronger increase in intensity of HREE solution complexation. These results show that the somewhat complex $\log {}_iK^{T}_{Fe}$ behavior shown in Fig. 1B has a relatively simple explanation in terms of competitive solution and surface complexation.

5. Summary

The present work describes the influence of carbonate complexation on YREE sorption by amorphous ferric hydroxide. In the absence of carbonate, YREE sorption is well explained by complexation of free trivalent YREEs (M^{3+}) at two surface sites (Quinn et al., 2006). When carbonate is added to the system, YREE sorption behavior is well described by adding only one new term to the surface complexation model that is appropriate in the absence of solution complexation. The new term accounts for sorption of YREE carbonate complexes (MCO_3^+) by amorphous ferric hydroxide. The YREE sorption model developed in this work (Eq. (12)), which incorporates the influences of both surface and solution complexation, quantitatively predicts (i) the increase in $\log {}_iK^{T}_{Fe}$ that is caused by an increase in pH, (ii) the increase in $\log {}_iK^{T}_{Fe}$ that occurs at low carbonate concentrations due to sorption of MCO_3^+ in addition to M^{3+}, and (iii) the decrease in $\log {}_iK^{T}_{Fe}$ that occurs at high carbonate concentrations, especially for HREEs, due to increasing solution complexation.

Acknowledgments

We thank the associate editor, Dr. K. H. Johannesson, for her skillful editorial handling of the manuscript. Additional thoughtful comments of Dr. W. M. Landing and an anonymous reviewer helped improve the manuscript. This work was supported by a grant from the National Science Foundation (OCE-0136333).

Associate editor: Karen Johannesson

Appendix A

See Tables A1–A7.

Table A1
Distribution coefficient ($\log {}_iK^{T}_{Fe}$) results from the experiment performed at pH 5.38 ± 0.02 and 30% CO_2

I (M)	0.0118	0.0118	0.0118	0.0118	0.0117	0.0117
pH	5.41	5.39	5.39	5.38	5.36	5.36
Time	15 min	90 min	5 h	24 h	46 h	48 h
CO_2 (%)	29.22	29.22	29.22	29.22	29.22	29.22
$[CO_3^{2-}]_T$ (μM)	0.0261	0.0238	0.0238	0.0227	0.0207	0.0207
Y	3.54	3.50	3.76	3.92	3.92	3.88
La	3.67	3.77	3.88	3.96	3.92	3.91
Ce	3.96	4.07	4.20	4.29	4.26	4.24
Pr	4.09	4.22	4.34	4.44	4.41	4.40
Nd	4.15	4.28	4.41	4.52	4.50	4.48
Pm	—	—	—	—	—	—
Sm	4.27	4.40	4.53	4.64	4.62	4.61
Eu	4.23	4.36	4.49	4.60	4.58	4.56
Gd	4.08	4.21	4.33	4.44	4.41	4.40
Tb	4.09	4.22	4.35	4.46	4.44	4.43
Dy	4.05	4.17	4.30	4.42	4.41	4.39
Ho	4.00	4.11	4.25	4.37	4.36	4.35
Er	4.00	4.12	4.26	4.39	4.38	4.37
Tm	4.06	4.19	4.34	4.47	4.47	4.45
Yb	4.10	4.23	4.38	4.52	4.52	4.51
Lu	4.08	4.22	4.37	4.51	4.51	4.49

Table A2
Distribution coefficient ($\log {}_iK^{T}_{Fe}$) results from the experiment performed over the pH range 4.6–6.6 at 3% CO_2

I (M)	0.0106	0.0106	0.0107	0.0109	0.0111	0.0116	0.0128
pH	4.63	4.98	5.49	5.70	5.99	6.28	6.60
Time	60 min	60 min	60 min	60 min	60 min	60 min	60 min
CO_2 (%)	2.904	2.904	2.904	2.904	2.904	2.904	2.904
$[CO_3^{2-}]_T$ (nM)	0.0693	0.347	3.65	9.64	36.9	142	638
Y	n.v.	n.v.	2.93	3.51	4.25	4.79	5.25
La	2.38	2.63	3.19	3.53	4.24	4.93	5.67
Ce	2.71	2.99	3.58	3.92	4.63	5.29	5.99
Pr	2.78	3.16	3.76	4.10	4.80	5.40	5.94
Nd	2.89	3.25	3.85	4.19	4.88	5.47	6.00
Pm	—	—	—	—	—	—	—
Sm	2.95	3.38	4.00	4.34	5.00	5.53	5.96
Eu	2.93	3.34	3.96	4.29	4.96	5.48	5.92
Gd	2.85	3.23	3.79	4.12	4.79	5.34	5.80
Tb	2.93	3.28	3.85	4.17	4.82	5.34	5.77
Dy	2.78	3.18	3.81	4.15	4.79	5.29	5.70
Ho	2.60	3.06	3.74	4.09	4.73	5.22	5.63
Er	2.60	3.09	3.78	4.12	4.75	5.22	5.61
Tm	2.67	3.17	3.88	4.22	4.83	5.27	5.63
Yb	2.81	3.28	3.97	4.30	4.89	5.30	5.65
Lu	2.74	3.25	3.94	4.27	4.88	5.30	5.64

It should be noted that carbonate concentrations ($[CO_3^{2-}]_T$) are listed in nM units. n.v., no value because measured YREE concentrations were indistinguishable from YREE concentrations at $t = 0$ (i.e., $[MS_i]_T = 0$ in Eq. (1)).

Table A3
Distribution coefficient ($\log {}_iK^{T}_{Fe}$) results from the experiment performed over the pH range 4.0–6.6 at 30% CO_2

I (M)	0.0106	0.0107	0.0109	0.0112	0.0120	0.0134	0.0162	0.0219	0.0342
pH	3.98	4.49	4.80	5.10	5.39	5.70	5.98	6.27	6.56
Time	60 min	60 min	60 min	60 min	60 min	60 min	60 min	60 min	60 min
CO_2 (%)	29.22	29.22	29.22	29.22	29.22	29.22	29.22	29.22	29.22
$[CO_3^{2-}]_T$ (nM)	0.0350	0.367	1.54	6.17	23.9	103	398	1680	7570
Y	n.v.	n.v.	2.55	3.19	3.70	4.24	4.70	4.97	5.07
La	2.10	2.59	2.87	3.25	3.71	4.36	5.03	5.48	5.91
Ce	2.34	2.71	3.13	3.56	4.04	4.66	5.26	5.72	6.04
Pr	2.42	2.97	3.30	3.72	4.21	4.78	5.32	5.68	5.91
Nd	2.49	3.04	3.36	3.79	4.28	4.83	5.35	5.70	5.93
Pm	—	—	—	—	—	—	—	—	—
Sm	2.30	3.13	3.47	3.91	4.40	4.92	5.40	5.71	5.88
Eu	2.39	3.11	3.45	3.88	4.36	4.87	5.33	5.62	5.76
Gd	2.35	2.95	3.30	3.72	4.19	4.73	5.22	5.53	5.69
Tb	2.39	3.03	3.34	3.77	4.22	4.73	5.18	5.47	5.59
Dy	2.19	2.96	3.32	3.74	4.19	4.67	5.10	5.35	5.44
Ho	2.05	2.92	3.27	3.70	4.14	4.62	5.04	5.28	5.35
Er	2.21	2.96	3.31	3.74	4.17	4.63	5.03	5.25	5.30
Tm	2.14	3.05	3.40	3.83	4.25	4.67	5.05	5.25	5.27
Yb	2.44	3.14	3.48	3.90	4.31	4.70	5.05	5.24	5.25
Lu	2.31	3.09	3.46	3.88	4.29	4.70	5.05	5.23	5.23

Table A4
Distribution coefficient ($\log {}_iK^{T}_{Fe}$) results from the experiment performed over the P_{CO_2} range 0–30% at pH 6.52 ± 0.01

I (M)	0.0107	0.0107	0.0107	0.0107	0.0107	0.0107	0.0107	0.0108	0.0108	0.0108	0.0109	0.0109	0.0109	0.0109	0.0110	0.0110	0.0110	0.0113	0.0113	0.0113	0.0124	0.0124	0.0124	0.0290	0.0290	0.0290
pH	6.51	6.53	6.54	6.50	6.52	6.54	6.56	6.52	6.53	6.53	6.54	6.52	6.52	6.52	6.52	6.52	6.52	6.52	6.51	6.51	6.53	6.52	6.51	6.51	6.51	6.51
Time	15 min	90 min	5 h	21 h	15 min	90 min	19 h	15 min	90 min	21 h	15 min	90 min	25 h	46.5 h	15 min	90 min	21.5 h	15 min	90 min	23 h	15 min	90 min	20.5 h	15 min	90 min	23.5 h
CO_2 (%)	0.0	0.0	0.0	0.0	0.00971	0.00971	0.00971	0.0969	0.0969	0.0969	0.291	0.291	0.291	0.291	0.485	0.485	0.485	0.961	0.961	0.961	2.904	2.904	2.904	29.22	29.22	29.22
$[CO_3^{2-}]_T$ (μM)	0.0	0.0	0.0	0.0	0.00140	0.00154	0.00168	0.0140	0.0147	0.0147	0.0463	0.0422	0.0422	0.0422	0.0705	0.0705	0.0705	0.141	0.134	0.134	0.458	0.437	0.417	5.63	5.63	5.63
Y	4.23	4.25	4.26	4.26	4.51	4.54	4.59	4.80	4.89	4.97	5.11	5.16	5.20	5.21	5.24	5.28	5.27	5.28	5.34	5.37	5.37	5.41	5.44	5.20	5.21	5.28
La	3.89	3.91	3.94	3.97	4.19	4.22	4.29	4.50	4.61	4.72	4.89	4.96	5.04	5.06	5.12	5.18	5.19	5.25	5.34	5.39	5.54	5.58	5.66	5.74	5.76	5.89
Ce	4.37	4.41	4.44	4.49	4.72	4.75	4.82	5.04	5.14	5.23	5.41	5.46	5.52	5.54	5.60	5.65	5.64	5.70	5.76	5.81	5.91	5.94	6.01	5.96	5.96	6.06
Pr	4.54	4.60	4.63	4.67	4.93	4.96	5.01	5.24	5.34	5.41	5.59	5.65	5.69	5.71	5.77	5.81	5.81	5.86	5.91	5.95	6.00	6.02	6.07	5.99	5.97	6.06
Nd	4.61	4.67	4.70	4.75	5.01	5.04	5.09	5.33	5.42	5.49	5.67	5.72	5.76	5.79	5.84	5.86	5.87	5.91	5.96	6.00	6.04	6.06	6.09	5.99	5.98	6.06
Pm	—	—	—	—	—	—	—	—	—	—	—	—	—	—	—	—	—	—	—	—	—	—	—	—	—	—
Sm	4.82	4.89	4.90	4.93	5.20	5.23	5.28	5.51	5.61	5.66	5.82	5.88	5.90	5.93	5.96	5.99	5.99	6.02	6.05	6.10	6.11	6.12	6.16	5.99	5.98	6.04
Eu	4.80	4.86	4.88	4.90	5.16	5.19	5.24	5.47	5.57	5.62	5.78	5.83	5.85	5.88	5.91	5.94	5.94	5.96	6.00	6.04	6.04	6.06	6.09	5.91	5.90	5.96
Gd	4.60	4.65	4.67	4.69	4.94	4.97	5.02	5.25	5.35	5.41	5.58	5.63	5.66	5.69	5.73	5.77	5.76	5.79	5.84	5.87	5.90	5.92	5.96	5.80	5.79	5.86
Tb	4.70	4.76	4.77	4.79	5.04	5.07	5.12	5.34	5.44	5.49	5.64	5.69	5.71	5.74	5.76	5.80	5.79	5.81	5.86	5.88	5.88	5.90	5.93	5.71	5.72	5.78
Dy	4.72	4.78	4.79	4.81	5.06	5.09	5.14	5.36	5.45	5.51	5.64	5.68	5.70	5.72	5.74	5.78	5.76	5.77	5.82	5.84	5.82	5.84	5.86	5.61	5.62	5.67
Ho	4.66	4.72	4.73	4.75	5.01	5.04	5.09	5.31	5.40	5.46	5.59	5.62	5.64	5.67	5.69	5.72	5.71	5.71	5.76	5.78	5.77	5.79	5.81	5.53	5.54	5.59
Er	4.69	4.75	4.76	4.78	5.05	5.08	5.13	5.34	5.43	5.50	5.62	5.65	5.68	5.70	5.71	5.75	5.74	5.73	5.77	5.80	5.77	5.78	5.80	5.49	5.49	5.54
Tm	4.79	4.86	4.87	4.90	5.17	5.20	5.25	5.46	5.55	5.61	5.71	5.75	5.76	5.79	5.79	5.82	5.81	5.80	5.84	5.86	5.82	5.83	5.84	5.50	5.51	5.53
Yb	4.89	4.96	4.98	5.01	5.28	5.32	5.37	5.56	5.66	5.70	5.79	5.82	5.84	5.87	5.86	5.89	5.87	5.85	5.88	5.91	5.83	5.85	5.86	5.48	5.49	5.51
Lu	4.85	4.91	4.92	4.95	5.23	5.26	5.32	5.52	5.61	5.66	5.75	5.79	5.80	5.84	5.83	5.86	5.85	5.82	5.86	5.88	5.82	5.83	5.84	5.45	5.46	5.48

Table A5
Distribution coefficient ($\log {}_iK^{T}_{Fe}$) results from the experiment performed over the P_{CO_2} range 0–30% at pH 6.68 ± 0.01

I (M)	0.0107	0.0107	0.0107	0.0107	0.0110	0.0110	0.0110	0.0111	0.0111	0.0111	0.0116	0.0115	0.0116	0.0133	0.0132	0.0132	0.0387	0.0386	0.0387
pH	6.65	6.68	6.71	6.68	6.68	6.67	6.69	6.68	6.67	6.68	6.69	6.67	6.68	6.70	6.69	6.69	6.69	6.68	6.69
Time	15 min	90 min	5 h	21.5 h	25 min	2 h	70 h	15 min	90 min	22 h	15 min	90 min	21.5 h	15 min	90 min	21 h	15 min	90 min	20.5 h
CO_2 (%)	0.0	0.0	0.0	0.0	0.291	0.291	0.291	0.485	0.485	0.485	0.961	0.961	0.961	2.904	2.904	2.904	29.22	29.22	29.22
$[CO_3^{2-}]_T$ (μM)	0.0	0.0	0.0	0.0	0.0884	0.0844	0.0925	0.148	0.141	0.148	0.310	0.282	0.296	1.02	0.974	0.974	14.5	13.8	14.5
Y	4.69	4.76	4.83	4.81	5.55	5.61	5.68	5.72	5.70	5.71	5.77	5.75	5.75	5.75	5.75	5.75	5.34	5.35	5.35
La	4.34	4.39	4.48	4.51	5.45	5.56	5.68	5.76	5.80	5.78	5.95	5.96	5.94	6.11	6.11	6.12	6.11	6.13	6.12
Ce	4.79	4.89	4.99	5.03	5.95	6.06	6.09	6.18	6.20	6.19	6.32	6.31	6.31	6.37	6.37	6.37	6.22	6.25	6.23
Pr	4.98	5.09	5.18	5.21	6.10	6.21	6.22	6.30	6.31	6.30	6.42	6.41	6.40	6.48	6.47	6.46	6.26	6.28	6.26
Nd	5.04	5.16	5.26	5.28	6.23	6.37	6.29	6.39	6.37	6.38	6.47	6.48	6.46	6.47	6.46	6.46	6.24	6.27	6.23
Pm	—	—	—	—	—	—	—	—	—	—	—	—	—	—	—	—	—	—	—
Sm	5.26	5.38	5.48	5.47	6.42	6.56	6.41	6.47	6.48	6.46	6.54	6.56	6.52	6.48	6.48	6.46	6.17	6.19	6.16
Eu	5.24	5.35	5.44	5.44	6.29	6.44	6.35	6.41	6.41	6.40	6.47	6.47	6.44	6.42	6.42	6.40	6.09	6.11	6.09
Gd	5.04	5.15	5.24	5.23	6.13	6.24	6.19	6.25	6.26	6.24	6.32	6.33	6.31	6.31	6.30	6.29	5.99	6.01	5.99
Tb	5.14	5.26	5.35	5.33	6.11	6.20	6.20	6.24	6.23	6.23	6.30	6.29	6.27	6.25	6.25	6.24	5.88	5.89	5.88
Dy	5.15	5.27	5.36	5.35	6.13	6.21	6.17	6.21	6.20	6.20	6.24	6.23	6.21	6.17	6.17	6.15	5.74	5.75	5.74
Ho	5.10	5.21	5.30	5.29	6.05	6.13	6.10	6.14	6.12	6.12	6.17	6.15	6.14	6.11	6.10	6.10	5.65	5.66	5.64
Er	5.13	5.25	5.33	5.32	6.10	6.18	6.12	6.16	6.13	6.13	6.17	6.16	6.15	6.09	6.08	6.08	5.59	5.59	5.58
Tm	5.23	5.35	5.44	5.44	6.24	6.32	6.20	6.23	6.21	6.21	6.23	6.22	6.21	6.12	6.11	6.11	5.57	5.57	5.56
Yb	5.33	5.47	5.56	5.56	6.22	6.31	6.23	6.25	6.23	6.23	6.24	6.23	6.21	6.13	6.12	6.11	5.54	5.54	5.53
Lu	5.28	5.41	5.51	5.50	6.15	6.23	6.21	6.22	6.20	6.21	6.22	6.20	6.20	6.11	6.11	6.10	5.51	5.51	5.49

Table A6
Distribution coefficient ($\log {}_iK^{T}_{Fe}$) results from the experiment performed over the P_{CO_2} range 0–30% at pH 7.06 ± 0.01

I (M)	0.0107	0.0107	0.0107	0.0107	0.0113	0.0113	0.0113	0.0117	0.0117	0.0117	0.0126	0.0125	0.0125	0.0167	0.0167	0.0167	0.0854	0.0844	0.0835
pH	7.04	7.06	7.08	7.05	7.07	7.08	7.07	7.06	7.06	7.07	7.06	7.04	7.04	7.07	7.06	7.06	7.07	7.06	7.05
Time	15 min	90 min	5 h	21 h	15 min	90 min	21.5 h	15 min	90 min	45 h	15 min	90 min	22.5 h	15 min	90 min	20 h	15 min	90 min	20.5 h
CO_2 (%)	0.0	0.0	0.0	0.0	0.291	0.291	0.291	0.485	0.485	0.485	0.961	0.961	0.961	2.904	2.904	2.904	29.22	29.22	29.22
$[CO_3^{2-}]_T$ (μM)	0.0	0.0	0.0	0.0	0.537	0.562	0.537	0.863	0.863	0.903	1.75	1.59	1.59	6.04	5.77	5.77	121	115	109
Y	5.48	5.63	5.68	5.70	6.10	6.18	6.20	6.12	6.19	6.13	6.07	5.99	6.08	5.82	5.90	5.85	4.69	4.73	4.71
La	5.10	5.25	5.31	5.37	6.27	6.37	6.39	6.45	6.51	6.49	6.52	6.37	6.56	6.47	6.46	6.52	6.58	6.69	6.75
Ce	5.62	5.80	5.88	5.97	6.86	6.94	7.01	7.01	7.11	7.06	7.04	6.85	7.06	6.81	6.88	6.91	6.44	6.53	6.57
Pr	5.83	5.99	6.06	6.05	6.81	6.88	6.94	6.91	6.98	6.93	6.91	6.79	6.93	6.71	6.79	6.77	6.55	6.61	6.60
Nd	5.91	6.09	6.16	6.22	6.91	7.02	7.12	7.01	7.10	7.10	7.02	6.90	7.06	6.77	6.85	6.83	6.51	6.61	6.56
Pm	—	—	—	—	—	—	—	—	—	—	—	—	—	—	—	—	—	—	—
Sm	6.16	6.34	6.39	6.45	7.00	7.09	7.16	7.07	7.14	7.10	7.02	6.92	7.02	6.73	6.85	6.77	6.30	6.39	6.32
Eu	6.12	6.30	6.34	6.39	6.86	6.94	6.97	6.90	6.96	6.91	6.85	6.77	6.87	6.61	6.70	6.65	6.16	6.24	6.19
Gd	5.92	6.09	6.13	6.18	6.77	6.86	6.92	6.81	6.92	6.83	6.79	6.68	6.80	6.54	6.62	6.56	6.05	6.13	6.08
Tb	6.03	6.19	6.24	6.28	6.71	6.79	6.83	6.74	6.80	6.74	6.68	6.60	6.68	6.41	6.50	6.44	5.83	5.91	5.86
Dy	6.02	6.18	6.24	6.28	6.62	6.70	6.71	6.62	6.69	6.61	6.54	6.47	6.56	6.26	6.35	6.29	5.61	5.68	5.62
Ho	5.93	6.09	6.15	6.19	6.49	6.57	6.60	6.49	6.57	6.51	6.44	6.37	6.44	6.14	6.24	6.17	5.45	5.53	5.45
Er	5.96	6.12	6.18	6.22	6.47	6.54	6.56	6.46	6.52	6.47	6.39	6.33	6.40	6.09	6.18	6.12	5.33	5.41	5.33
Tm	6.07	6.24	6.30	6.35	6.53	6.59	6.63	6.51	6.58	6.52	6.43	6.37	6.43	6.09	6.20	6.13	5.27	5.34	5.28
Yb	6.18	6.35	6.44	6.49	6.56	6.64	6.68	6.54	6.61	6.55	6.45	6.38	6.45	6.08	6.18	6.11	5.21	5.28	5.22
Lu	6.13	6.31	6.38	6.42	6.54	6.61	6.65	6.51	6.59	6.54	6.43	6.37	6.43	6.05	6.16	6.09	5.16	5.23	5.16

Table A7
Distribution coefficient ($\log K^{T}_{Fe}$) results from the experiment performed over the P_{CO_2} range 0–30% at pH 7.10 ± 0.03

I (M)	0.0105	0.0105	0.0105	0.0105	0.0105	0.0105	0.0105	0.0112	0.0112	0.0112	0.0116	0.0116	0.0116	0.0127	0.0127	0.0127	0.0176	0.0175	0.0175	0.0811	0.0811	0.0940	0.0930
pH	7.12	7.13	7.15	7.13	7.08	7.10	7.07	7.10	7.11	7.11	7.10	7.10	7.10	7.11	7.10	7.10	7.13	7.12	7.12	7.04	7.04	7.11	7.10
Time	15 min	90 min	5 h	22 h	15 min	90 min	22.5 h	65.5 h	15 min	90 min	21.5 h	15 min	90 min	22 h	15 min	90 min	21 h	15 min	90 min	19.5 h	15 min	2.5 h	19 h	15 min	90 min
CO_2 (%)	0.0	0.0	0.0	0.0	0.00971	0.00971	0.00971	0.00971	0.291	0.291	0.291	0.485	0.485	0.485	0.961	0.961	0.961	2.904	2.904	29.22	29.22	29.22	29.22	29.22	29.22
$[CO_3^{2-}]_T$ (μM)	0.0	0.0	0.0	0.0	0.0167	0.0184	0.0201	0.0175	0.614	0.643	0.643	1.03	1.03	1.03	2.20	2.11	2.11	8.10	7.72	7.72	103	103	152	152	145
Y	5.61	5.80	5.84	5.84	5.97	6.02	6.06	5.96	6.10	6.15	6.15	6.16	6.11	6.15	6.09	6.11	6.07	5.91	5.89	5.88	4.69	4.62	4.61	4.51	4.48
La	5.26	5.47	5.57	5.57	5.82	5.85	5.90	5.80	6.28	6.38	6.46	6.50	6.42	6.51	6.55	6.54	6.48	6.53	6.45	6.45	6.60	6.53	6.57	6.58	6.56
Ce	5.77	6.01	6.14	6.16	6.35	6.39	6.44	6.36	6.81	6.96	6.91	7.01	6.90	7.04	7.08	7.08	7.01	6.77	6.71	6.74	6.43	6.38	6.42	6.35	6.32
Pr	5.95	6.18	6.32	6.32	6.48	6.53	6.60	6.52	6.74	6.81	6.85	6.87	6.83	6.87	6.87	6.86	6.82	6.79	6.74	6.75	6.58	6.52	6.53	6.46	6.45
Nd	6.03	6.27	6.41	6.41	6.58	6.60	6.70	6.63	6.77	6.85	6.87	6.89	6.84	6.90	6.88	6.88	6.86	6.76	6.73	6.73	6.51	6.44	6.46	6.37	6.36
Pm	—	—	—	—	—	—	—	—	—	—	—	—	—	—	—	—	—	—	—	—	—	—	—	—	—
Sm	6.23	6.49	6.68	6.69	6.77	6.83	6.91	6.84	6.88	6.97	6.96	6.97	6.93	6.99	6.96	6.95	6.89	6.72	6.69	6.72	6.33	6.28	6.29	6.19	6.17
Eu	6.22	6.50	6.71	6.70	6.81	6.87	6.98	6.88	6.82	6.90	6.91	6.90	6.85	6.91	6.87	6.88	6.82	6.62	6.59	6.61	6.22	6.15	6.16	6.06	6.04
Gd	6.04	6.29	6.46	6.45	6.58	6.63	6.72	6.61	6.66	6.73	6.75	6.75	6.72	6.75	6.72	6.72	6.67	6.49	6.45	6.46	6.08	6.01	6.01	5.92	5.90
Tb	6.11	6.34	6.48	6.48	6.56	n.v.	6.69	6.59	6.61	6.68	6.68	6.67	6.64	6.67	6.62	6.64	6.59	6.40	6.39	6.39	5.90	5.82	5.82	5.71	5.70
Dy	6.11	6.34	6.45	6.47	6.54	6.58	6.66	6.56	6.59	6.64	6.65	6.62	6.58	6.62	6.56	6.56	6.52	6.33	6.30	6.31	5.70	5.62	5.60	5.49	5.48
Ho	6.06	6.28	6.36	6.37	6.45	6.52	6.58	6.48	6.47	6.52	6.51	6.50	6.46	6.49	6.43	6.45	6.40	6.22	6.20	6.21	5.54	5.44	5.43	5.31	5.30
Er	6.08	6.29	6.37	6.38	6.45	6.52	6.58	6.48	6.47	6.51	6.50	6.48	6.44	6.48	6.40	6.41	6.38	6.18	6.16	6.16	5.42	5.33	5.31	5.18	5.17
Tm	6.18	6.39	6.46	6.48	6.53	6.61	6.67	6.58	6.54	6.57	6.56	6.54	6.49	6.53	6.44	6.45	6.41	6.18	6.16	6.15	5.35	5.26	5.24	5.11	5.10
Yb	6.27	6.50	6.58	6.61	6.62	6.72	6.77	6.69	6.53	6.57	6.56	6.53	6.48	6.52	6.42	6.43	6.39	6.14	6.13	6.13	5.29	5.20	5.18	5.05	5.04
Lu	6.22	6.44	6.50	6.54	6.58	6.65	6.72	6.63	6.51	6.54	6.54	6.50	6.45	6.49	6.39	6.40	6.37	6.12	6.10	6.10	5.23	5.14	5.12	4.99	4.98

n.v. = no value because of an anomalous concentration reading.

References

Bau, M., 1999. Scavenging of dissolved yttrium and rare earths by precipitating iron oxyhydroxide: experimental evidence for Ce oxidation, Y–Ho fractionation, and lanthanide tetrad effect. *Geochim. Cosmochim. Acta* **63** (1), 67–77.

Bingler, L.S., Byrne, R.H., Vargo, G.A., Tomas, C.R., 1989. Rare earth element uptake by the marine diatom *Skeletonema costatum*. *Chem. Spec. Bioavailab.* **1** (3), 103–110.

Byrne, R.H., Kim, K.-H., 1990. Rare earth element scavenging in seawater. *Geochim. Cosmochim. Acta* **54**, 2645–2656.

Byrne, R.H., Sholkovitz, E.R., 1996. Marine chemistry and geochemistry of the lanthanides. In: Gschneidner, K.A. Jr., Eyring, L. (Eds.), *Handbook on the Physics and Chemistry of Rare Earths*, vol. 23. Elsevier, Amsterdam, pp. 497–593.

Davranche, M., Pourret, O., Gruau, G., Dia, A., 2004. Impact of humate complexation on the adsorption of REE onto Fe oxyhydroxide. *J. Colloid Interf. Sci.* **277**, 271–279.

De Carlo, E.H., Wen, X.-Y., Irving, M., 1998. The influence of redox reactions on the uptake of dissolved Ce by suspended Fe and Mn oxide particles. *Aquat. Geochem.* **3**, 357–389.

Dzombak, D.A., Morel, F.M.M., 1990. *Surface Complexation Modeling. Hydrous Ferric Oxide*. John Wiley & Sons, New York.

Fairhurst, A.J., Warwick, P., Richardson, S., 1995. The influence of humic acid on the adsorption of europium onto inorganic colloids as a function of pH. *Colloids Surfaces A. Physicochem. Eng. Aspects* **99**, 187–199.

Ferri, D., Grenthe, I., Hietanen, S., Salvatore, F., 1983. Studies on metal carbonate equilibria. 5. The cerium(III) carbonate complexes in aqueous perchlorate media. *Acta Chem. Scand. A* **37**, 359–365.

Hayes, K.F., Leckie, J.O., 1987. Modeling ionic strength effects on cation adsorption at hydrous oxide/solution interfaces. *J. Colloid Interf. Sci.* **115** (2), 564–572.

Kawabe, I., Ohta, A., Ishii, S., Tokumura, M., Miyauchi, K., 1999a. REE partitioning between Fe–Mn oxyhydroxide precipitates and weakly acid NaCl solutions: convex tetrad effect and fractionation of Y and Sc from heavy lanthanides. *Geochem. J.* **33**, 167–179.

Kawabe, I., Ohta, A., Miura, N., 1999b. Distribution coefficients of REE between Fe oxyhydroxide precipitates and NaCl solutions affected by REE-carbonate complexation. *Geochem. J.* **33**, 181–197.

Koeppenkastrop, D., De Carlo, E.H., 1992. Sorption of rare-earth elements from seawater onto synthetic mineral particles: an experimental approach. *Chem. Geol.* **95**, 251–263.

Koeppenkastrop, D., De Carlo, E.H., 1993. Uptake of rare earth elements from solution by metal oxides. *Environ. Sci. Technol.* **27** (9), 1796–1802.

Koeppenkastrop, D., De Carlo, E.H., Roth, M., 1991. A method to investigate the interaction of rare earth elements in aqueous solution with metal oxides. *J. Radioanal. Nucl. Chem. Art.* **152** (2), 337–346.

Liu, X., Byrne, R.H., 1998. Comprehensive investigation of yttrium and rare earth element complexation by carbonate ions using ICP-mass spectrometry. *J. Sol. Chem.* **27** (9), 803–815.

Liu, X., Millero, F.J., 1999. The solubility of iron hydroxide in sodium chloride solutions. *Geochim. Cosmochim. Acta* **63** (19/20), 3487–3497.

Luo, Y.-R., Byrne, R.H., 2004. Carbonate complexation of yttrium and the rare earth elements in natural waters. *Geochim. Cosmochim. Acta* **68** (4), 691–699.

Marmier, N., Fromage, F., 1999. Comparing electrostatic and nonelectrostatic surface complexation modeling of the sorption of lanthanum on hematite. *J. Colloid Interf. Sci.* **212**, 252–263.

Ohta, A., Kawabe, I., 2000. Rare earth element partitioning between Fe oxyhydroxide precipitates and aqueous NaCl solutions doped with $NaHCO_3$: determinations of rare earth element complexation constants with carbonate ions. *Geochem. J.* **34**, 439–454.

Ohta, A., Kawabe, I., 2001. REE(III) adsorption onto Mn dioxide (δ-MnO_2) and Fe oxyhydroxide: Ce(III) oxidation by δ-MnO_2. *Geochim. Cosmochim. Acta* **65** (5), 695–703.

Quinn, K.A., Byrne, R.H., Schijf, J., 2004. Comparative scavenging of yttrium and the rare earth elements in seawater: competitive influences of solution and surface chemistry. *Aquat. Geochem.* **10**, 59–80.

Quinn, K.A., Byrne, R.H., Schijf, J., 2006. Sorption of yttrium and rare earth elements by amorphous ferric hydroxide: influence of pH and ionic strength. *Mar. Chem.* **99**, 128–150.

Rabung, T., Geckeis, H., Kim, J.-I., Beck, H.P., 1998a. Sorption of Eu(III) on a natural hematite: application of a surface complexation model. *J. Colloid Interf. Sci.* **208**, 153–161.

Rabung, T., Geckeis, H., Kim, J.I., Beck, H.P., 1998b. The influence of anionic ligands on the sorption behaviour of Eu(III) on natural hematite. *Radiochim. Acta* **82**, 243–248.

Stanley Jr., J.K., Byrne, R.H., 1990. The influence of solution chemistry on REE uptake by *Ulva lactuca* L. in seawater. *Geochim. Cosmochim. Acta* **54**, 1587–1595.

Swallow, K.C., Hume, D.N., Morel, F.M.M., 1980. Sorption of copper and lead by hydrous ferric oxide. *Environ. Sci. Technol.* **14** (11), 1326–1331.

Tang, J., Johannesson, K.H., 2005. Adsorption of rare earth elements onto Carrizo sand: experimental investigations and modeling with surface complexation. *Geochim. Cosmochim. Acta* **69** (22), 5247–5261.

Wood, S.A., 1990. The aqueous geochemistry of the rare-earth elements and yttrium. 1. Review of available low-temperature data for inorganic complexes and the inorganic REE speciation of natural waters. *Chem. Geol.* **82**, 159–186.